Energy Management for Indoor Hovering Robots

James F. Roberts, Jean-Christophe Zufferey and Dario Floreano (Pre-print version, Published at IROS2008)

***Abstract*— Flying has an advantage when compared to ground based locomotion, as it simplifies the task of overcoming obstacles and allows for rapid coverage of an area while also providing a birds-eye-view of the environment. One of the key challenges that has prevented engineers from coming up with convincing aerial solutions for indoor exploration is the energetic cost of flying. This paper presents a way of mitigating the energy problem regarding aerial exploration within indoor environments. This is achieved by means of a model to estimate the endurance of a hover-capable flying robot and by using ceiling attachment as a means of preserving energy while maintaining a birds-eye-view. The proposed model for endurance estimation has been extensively tested using a custom-developed quadrotor and autonomous ceiling attachment system.**

I. CHALLENGES AND STATE OF THE ART

The idea of using flying robots to explore indoor environments has become popular within the robotic community in recent times [1], [2], [3], [4], [5] [1] [2]. Flying has an advantage when compared to ground based locomotion, as it simplifies the task of overcoming obstacles and allows for rapid coverage of an area while also providing a birds-eye-view of the environment. One of the key challenges that has prevented engineers from coming up with convincing aerial solutions for indoor exploration is the energetic cost of flying, which is orders of magnitude higher than that of terrestrial locomotion.

Imagine a robot that can fly around indoors, its task is to search a building for a pre-defined target, for example an injured human. It flies into a room and uses its on-board thermal vision sensors to scan the room for the injured human. After finding no positive matches the robot flies into the next room. The robot searches three rooms in this manner and locates the injured human in the last room. The robot has a limited amount of energy. If the robot was required to search more than these three rooms, then it is likely that its limit is reached before finding its target. If the robot could attach to the ceiling while it is searching the room, instead of remaining airborne, the search could be extended from minutes to hours, which could make all the difference in such a situation.

Valenti and collaborators have developed a health management system to aid online mission planning for swarms of hovering Unmanned Air Vehicles (UAV) [6]. They have found that it is possible to estimate the remaining flight endurance by comparing the platforms battery voltage and collective stick position over time. The initative for doing this was to aquire information about the health of the platform and possible detection of faults. Their testing results show that the comparison between the predicted and actual remaining flight time varies by the order of two minutes.

Laboratory of Intelligent Systems (LIS), Ecole Polytechnique Fédérale de Lausanne (http://lis.epfl.ch), Lausanne, 1015, Switzerland. james.roberts@epfl.ch

[1] http://www.swarmanoid.org

[2] http://www.mufly.ethz.ch

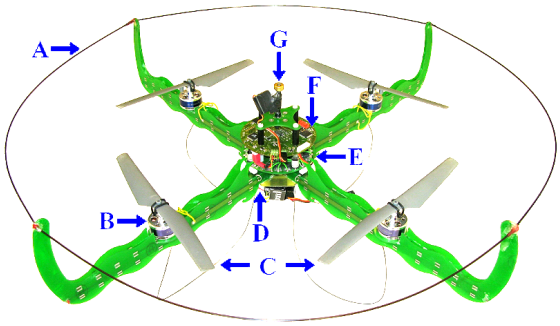

Fig. 1. The PCB quadrotor platform: A) protection ring, B) brushless motor, C) contra-rotating propellers, D) LIPO battery, E) high-speed motor controller, F) flight computer, G) ceiling attachment

This paper tackles the energy problem of aerial exploration within indoor environments, first by using ceiling attachment as a means for preserving energy, while still maintaining the birds-eye-view and second by providing an estimation model to estimate the endurance of a hover-capable flying robot. The proposed model for endurance estimation has been extensively tested using a custom-developed quadrotor and ceiling attachment system (Fig. 1). The ceiling attachment feature has been successfully demonstrated by autonomously flying through several cycles of hovering, attaching to the ceiling, powering off the motors and waiting, re-activating the motors and autonomousy detaching from the ceiling.

In the following section, we present the platform, its structure, propulsion system, ceiling attachment device and avionics. We then introduce the endurance estimation model and precisely test it in a number of indoor flights with and without ceiling attachment.

II. PLATFORM

A. Structure

The custom-built platform (Fig. 1) is based on a conventional quadrotor design with some structural modifications. The idea is to have a tight integration between the structure, electronics and sensors to reduce weight, minimise wiring, and improve manufacturability. A good material for structure fabrication is FR4 Printed Circuit Board (PCB). The PCB body is extended out to support a carbon fibre ring. This simple ring allows the platform to survive small

collisions with the surrounding environment such as walls and ceiling without causing damage to either the platform or the obstacles. The system is designed so that additional control boards and/or sensors can be stacked in its centre with minimal effort. The total weight of the structure, including the embedded electronics, without the battery, is 416 g.

B. Propulsion

The propulsion system consists of two pairs of brushless out-runner motors, each pair fitted with 200 mm contra-rotating plastic propellers, which are powered by a 3-cell 2100 mAh Lithium Polymer (LiPo) battery (weighing 144 g). This configuration provides 2.55 N ($\sim$260 g) of thrust, at the maximum battery voltage for each motor, giving a total thrust of 10.2 N ($\sim$1040 g).

C. Ceiling Attachment

Attachment to a ferrous ceiling is achieved by using a small toroidal magnet with an attractive force of $\sim$24.5 N (2500 g). The ceiling attachment device is located centrally at the top of the structure (Fig. 2). In the future more universal systems, such as dry adhesives [7], [8], [9], [10], will be evaluated to attach to non-ferrous ceilings, however, the main goal in this paper is to explore the new concept of ceiling attachment for extended autonomous operation. By using a magnetic system we have greatly simplified the task of attaching to the ceiling. A passive system like this allows the platform to remain attached to the ceiling while consuming minimal energy. To detach from the ceiling a mechanical lever pushes a carbon fiber rod through the center of the toroid. With the rod protruding only 5 mm the weight of the platform is sufficient to cause a detach and allow the platform to continue flying. The lever is activated by a micro-servo that is directly controlled by the flight computer. To detect when a ferrous ceiling is present, a hall-effect sensor has been placed perpendicular with the toroidal magnet. The magnetic coupling, when the sensor comes near a ferrous object, gives an indication on weather the ceiling attachment device has a connection. A sweeping like search method could be employed for roofs that only have small metalic surfaces to attach to, for example sparsely spaced bolts. The attachment method is still viable, however, much time would be wasted in searching for a good/possible connection.

D. Avionics

The quadrotor is naturally a highly non-linear and unstable platform which requires six Degree of Freedom (DOF) inertial sensing and stability controllers to deal with its fast dynamics. For this purpose we have developed a custom flight computer and adapted a high-speed brushless motor controller developed by Mikrokopter[3].

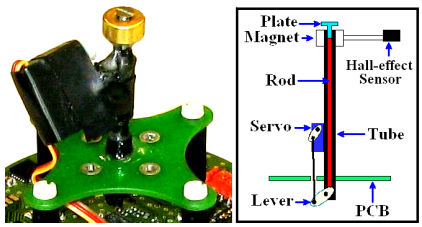

Fig. 2. The ceiling attachment/detachment device is mounted centerally on top of the platform.

The high-speed brushless motor controller enables each of the four motors to be updated at a rate of 500 Hz through an I^2C interface. This allows for a high update rate of the entire stability control system, from sensor to actuator. By sampling at an update rate an order of magnitude higher than the bandwidth of the gyroscopes (50 Hz) the response is fast enough to stabilise the non-linear dynamics of the system using simple controllers.

The flight computer [11] incorporates most of the sensors. The euler angles of the system are estimated using complimentary filtered, inertial information from three rate gyroscopes and three accelerometers. Stability control of roll and pitch is achieved using two proportional-integral-derivative controllers. A simple proportional controller is implemented for yaw stabilisation. The altitude of the platform is measured using an ultrasonic sensor aimed towards the ground, which is capable of measuring up to 6.4 m with a resolution of 2.54 cm (for more details on previous work with fully autonomous flight control please refer to [11]). These simple sensors and control methods are enough to allow for autonomous ceiling attachment/detachment, however, at this stage commands for position control in the pitch, roll and yaw rotations are given by a safety pilot.

III. ENDURANCE ESTIMATION

In order to calculate the estimated flight endurance we make the assumption that when the platform is flying the thrust is equal to its own weight. It is also assumed that the fluctuations in the control response average to a constant value and are equal to the static test case. First the motor and propeller setup is characterised to determine the systems relationship between power consumption and thrust. Then, based on this characterisation, an estimation model is used to deduce the estimated flight endurance using the total take-off weight and the battery capacity. The estimation model can also deal with variations in payload mass, payload power consumption and idle state power consumption. With this method the performance of future battery technologies can also be estimated based on the specific energy density of the technology. This estimation model is then used to find the best battery for our quadrotor system by performing an optimal search from a list of avaliable batteries. The estimation model is then adapted to incorporate the ceiling attachment system, which can be used to estimate the remaining endurance avaliable to the robot while attached to the ceiling.

A. Endurance Estimation Model

Generally speaking, we can apply this endurance model to various different hovering platforms by manipulating the motor power input parameter, without having to know

[3]http://www.mikrokopter.com

anything about the discharge characteristics of the battery. In order to calculate the estimated flight endurance t^E we first need to define all the affecting parameters including the total take-off weight m^T, total idle-state power consumption p^I and battery capacity c^B (W.h). These parameters can then be used to determine the estimated flight endurance t^E, with the possibility for variations in the battery capacity c^B, payload mass m^P payload power consumption p^P and the thrust vs motor power curve (Fig. 3).

The total take-off weight m^T is obtained by summing the individual component masses of the structure m^S, battery m^B and payload m^P:

$$m^T = m^S + m^B + m^P, \tag{1}$$

Similarly, the total idle-state power consumption p^I is a summation of the avionics p^A and payload power p^P consumptions:

$$p^I = p^A + p^P, \tag{2}$$

The battery capacity can be defined by its specific energy density e^D (W.h/kg) and relative mass m^B:

$$c^B = e^D \cdot m^B, \tag{3}$$

The estimated flight endurance t^E can then be expressed as:

$$t^E = c^B/(p^M + p^I), \tag{4}$$

where p^M is the motor power taken from the thrust curve (Fig. 3) at the point where the thrust is equal to the total take-off weight m^T of the platform.

There is one major limitation, with respect to the battery voltage, that needs to be taken into account. As the battery voltage reduces during the flight there is also a relative reduction in the avaliable thrust. Therefore, it is necessary to take a measurement of the motor thrust limit m^L when the battery is at its minimum voltage. This can be done with a motor test-rig by setting the power supply to the minimum battery voltage and recording the thrust. This thrust measurement allows us to calculate the maximum payload mass limit m^X:

$$m^X = m^L - m^T, \tag{5}$$

B. Endurance Estimation with Ceiling Attachment

By using the ceiling attachment capability the endurance can be easily extended from minutes to hours. However, it is important to leave some reserved energy for the platform to detach, fly back and land safely. While the platform is attached to the ceiling it continues to consume power at a rate determined by the idle-state power consumption. This introduces an interesting situation when the ceiling attachment capability is used as the flight times can not simply be added together. One might want to estimate the remaining time that the system will operate while attached to the ceiling. One might also want to estimate the reserved energy in order to determine the flight endurance after being attached for a given time.

From equation (4) the estimated ceiling endurance t^C can be calculated without the influence of the motor power consumption:

$$t^C = c^B/p^I, \tag{6}$$

The reserved endurance energy ratio r^E can then be represented as a ratio between the original estimated flight endurance t^E and the elapsed flight time t^F:

$$r^E = (t^E - t^F)/t^E, \tag{7}$$

This allows us to calculate the reserved endurance at the exact moment the platform attaches to the ceiling. The reserved endurance energy ratio r^E can then be modified to take into account the time that the platform is attached to the ceiling. This has been defined as the post ceiling endurance energy ratio r^{Ep}, which is the remaining endurance power ratio after an elapsed attachment time t^A:

$$r^{Ep} = r^E - (t^E \cdot t^A/t^C), \tag{8}$$

The reserved endurance t^R, which takes into account the elapsed flight time t^F and the elapsed attachment time t^A, can then be calculated using equation (8):

$$t^R = c^B \cdot r^{Ep}/(p^M + p^I), \tag{9}$$

C. Static Thrust Measurement

A custom test-rig has been created to measure the thrust and power consumption of the motor-propeller system. This simple test-rig consists of an aluminium motor mount, motor speed controller, current & voltage meters and weight balance. The motor is fixed to the motor-mount and then both are attached to the weight balance. By attaching the rig directly to the weight balance the thrust can be easily read from the meter (after zeroing the setup's mass). A

high current DC power supply can be used to help regulate the input power and keep the results more consistent. The current and voltage meters are used to determine the power consumption. Samples of the current and voltage are then taken at regular thrust increments depending on the desired resolution. The propeller mounting was inverted to prevent any ground effect errors cased by downwash.

Our motor-propeller system has been characterised using the procedure above. Samples of the current and voltage were taken at ten-gram thrust increments. The motor-propeller system characterisation can be seen in Fig. 3. In our case we used a fifth order polynomial fitting function to smooth out the measured response. For our quadrotor platform, the motor power is taken from the thrust curve at the point where the thrust is equal to a quarter of the total take-off weight. This is due to the fact that we have four propulsion systems lifting the same body mass. The motor power from the thrust curve p^M is then multiplied by 4 to obtain the correct motor power p^M for all four motors.

Our platform has an automatic landing feature that is triggered when the flight computer detects that the battery is at the minimum battery voltage. This feature is used to prevent damage to the battery, increase the safety for both the pilot and the platform by preventing critical battery voltages and allows for accurate endurance timing during experiments. The voltage for battery cut-off is set at 3.0 V per cell. Therefore, if the battery voltage goes below 9.0 V the automatic land feature is activated and the platforms thrust reduced in software.

With each charge and discharge cycle a batteries holding capacity will slowly reduce. This effect can be minimised by preventing the cell voltage to drop below this 3.0 V minimum. At this stage the proposed model does not yet include battery degradation. Further studies on this topic would be required to determine where a significant effect on the estimated flight endurance starts to occur. In the future it would be possible to design a small circuit board that is permanently fitted to the battery. This would house a small microcontroller running the proposed model as an online estimation algorithm. Information about the platform could be communicated to the device in order to accurately determine that platforms particular flight time. An algorithm could then be used to adjust the estimation for battery degradation based on the error between the estimated and actual measured flight endurance.

D. Battery Selection Optimisation

In order to maximise the flight endurance of the platform we need to find the optimum battery. To find the optimum battery we can use the estimation model (4) with an optimal search to find the optimum battery weight for a given platform, based on its specific thrust, power and weight properties. We can see in Figure 4 that there is an optimal point where the flight endurance is maximsed. This point can be refered to as the 'ideal battery optimum' as it shows the endurance for an ideal battery that supplies a constant voltage until the battery energy is depleted. However, to

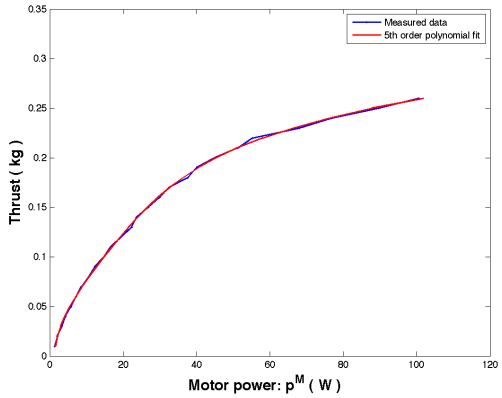

Fig. 3. Thrust curve of the motor-propeller system showing the power required for a certain hover thrust (taken at a nominal voltage of 12.5 V).

obtain the 'realistic battery optimum' for a battery thats voltage reduces as the battery energy is drained, we apply the maximum payload limit (5). This limit can be seen in Fig. 4, labled as the 'realistic battery optimum'. From the output of the optimisation function we obtain the optimal ideal battery mass, m^B=0.353 kg, and the optimal realistic battery mass, m^B=0.169 kg. This relates to a predicted endurance of t^E=19.76 min, and t^E=15.28 min, respectively.

It is possible to use this optimisation method to automatically select the best suited battery from a list of battery packs avaliable on the market. This is done by first creating a list of the battery specifications which must include the specific energy density and the battery mass as given by the manufacture. The optimisation method above is then performed on each of the batteries in the list. After doing this for every battery, the list can then be sorted in order of flight endurance, where the battery with the highest endurance is the optimal battery for the system.

For our platform we created a list of thirty three different 3-cell battery packs that are avaliable online. The sorted list

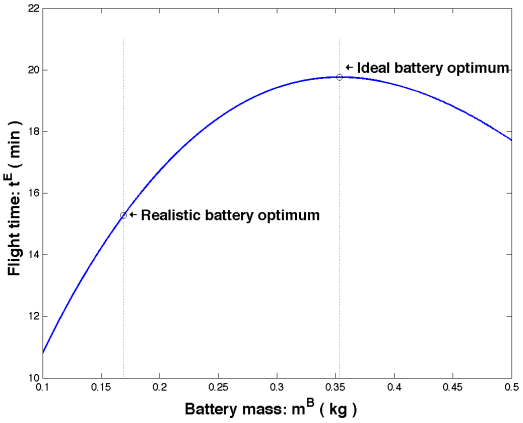

Fig. 4. Flight time vs battery mass according to Equ. 3, 4 & 5 allow for finding the optimum battery mass for our quadrotor without additional payload (m^S=0.431 kg, m^P=0 kg, p^A=2.44 W, p^P=0 W, e^D=164 W.h/kg)

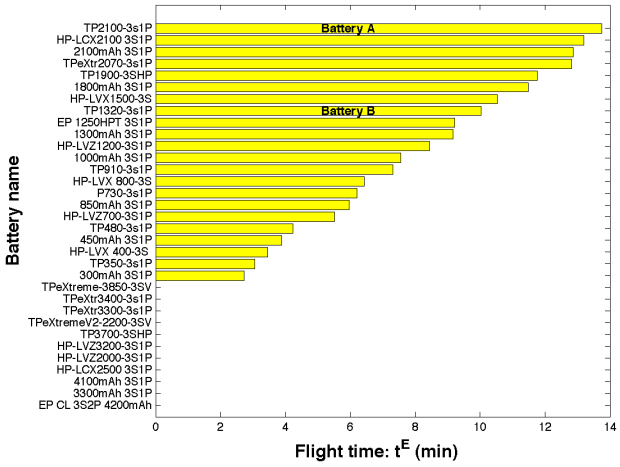

Fig. 5. List of battery packs sorted by flight endurance according to Equ. 4 & 5. Battery A & B will be used for testing, Battery-A = TP-2100-3S1P, Battery-B = TP-1320-3S1P (m^S=0.431 kg, m^P=0 kg, p^A=2.44 W, p^P=0 W)

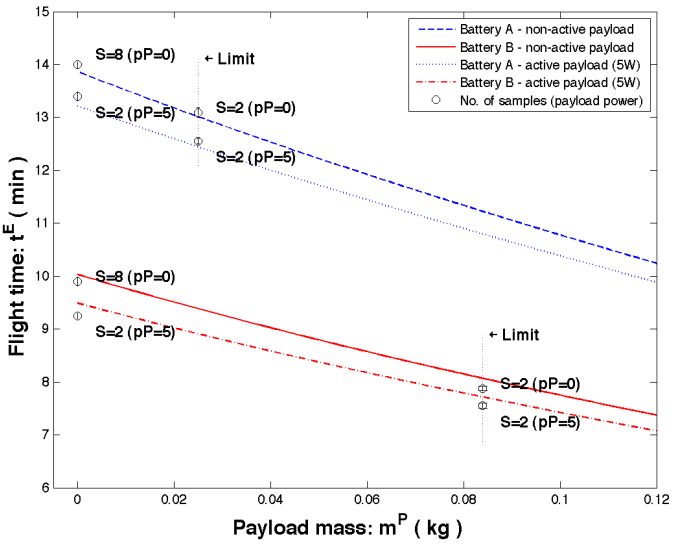

Fig. 6. Estimated and measured endurance for variable payloads and active payload power consumptions. The top pair of lines and the bottom pair of lines represent the estimated flight endurance of Battery-A and Battery-B, respectively. The higher line and the lower line of each pair represents the non-active and active payloads, respectively. Error bars have been plotted on each sample point marked by a circle (m^S=0.431 kg, p^A=2.44 W, m^B(Battery-A)=0.144 kg, e^D(Battery-A)=172 W.h/kg, m^B(Battery-B)=0.085 kg, e^D(Battery-B)=164 W.h/kg).

in Figure 5 shows the optimal battery is the 'TP-2100-3S1P' which we have defined as 'Battery-A'. Any battery that does not meet the payload limit has its respective endurance set to zero.

IV. IN-FLIGHT EXPERIMENTS

The goal of these experiments is to test the flight endurance estimation model with variations in payload mass, payload power consumption and time spent attached to the ceiling.

We present two experiments that show the progression towards achieving this goal. The first experiment was designed to observe the accuracy of the estimations for variations in payload mass and payload power consumption with two different battery sizes and the second experiment was designed to observe the accuracy of the estimations for a scenario with multiple autonomous attachments and detachments, which is much like the scenario in the introduction.

A. Experiment 1: Endurance Test

In the first experiment, the platform was flown under manual control and a stop watch was used to time the flight endurance. Battery-A (m^B=0.144 kg, e^D=164 W.h/kg) was chosen because it is the optimal battery for the system, without payload, and Battery-B (m^B=0.085 kg, e^D=172 W.h/kg) was chosen because it is in the middle range (see Fig. 5).

The estimated flight endurance over the full range of payload has been plotted for both batteries each with and without an active payload of 5 W (Fig. 6). In order to see the realistic range of endurance estimations the maximum payload limits, obtained using equation (5), have been plotted. Samples have been taken first at the minimum and maximum payload points without a payload power consumption and then, at the minimum and maximum payload points with a 5 W payload power consumption. For the no-payload test cases a set of eight flight time samples were taken for two different battery sizes, however, due to the large amount of time required to do the extra 48 test flights, only two samples have been taken for the other test cases. We assume that these two samples are a reasonable representation of the actual measured mean endurance. We also assume that if the minimum and maximum payload limits are reasonable then any measurement between these points are also representative.

The error bars have been plotted on Fig. 6. We can see that for both battery sizes the estimated flight endurance is accurate, the samples have a maximum mean error of only 2.52 %. These results suggest that the power model for flight endurance estimation for both payload mass and payload power consumption is realistic and that the assumptions are reasonable.

B. Experiment 2: Ceiling Endurance Test

In the second experiment, the task is to test the ceiling endurance estimation. The robot was commanded to fly through several cycles of hovering, attaching to the ceiling, powering off the motors and waiting, re-activating the motors and detaching from the ceiling. This is to simulate the scenario in the introduction where the robot is scanning multiple rooms for a target. The altitude log for a single autonomous ceiling attachment/detachment cycle can be seen in Fig. 7. The robot performs an automatic take-off from the ground and hovers at the pre-defined altitude of 1 m. A command is wirelessly sent to the robot to initiate a ceiling attachment, the altitude is then slowly increased until the robot is attached to the ceiling at 2.5 m. The hall-effect sensor is then used to determine if the robot has a good connection and then the motors are powered down. After receiving the detach command the robot reactivates the motors, detaches

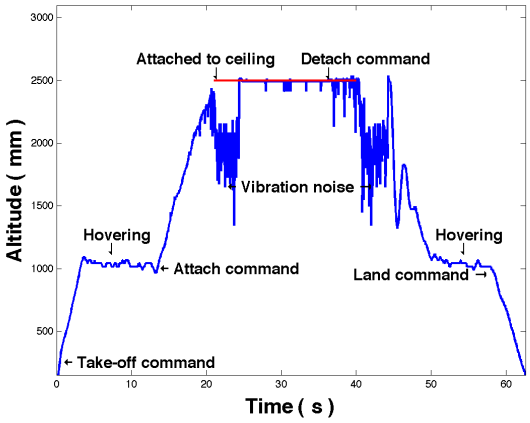

Fig. 7. Altitude log during a single autonomous ceiling attachment/detachment cycle.

TABLE I

RESULTS FROM EXPERIMENT 2:

Battery	Estimated (min)	Mean (STD) (min)	Error (%)	Samples
Battery-A	103.3	102.3 (0.2)	0.97	2

from the ceiling and returns to the pre-defined hovering altitude, the robot then performs an automatic landing on the ground.

The hovering time and attached time are defined as 2 min and 30 min, respectively. This cycle was repeated three times, giving a total elapsed flying time t^F of 6 min and a total elapsed attached time t^A of 90 min. The time from the last detachment until the battery was depleted was then recorded.

Using the endurance models for both the hovering case and the attached case, we can estimate the total flight endurance to be 103 min (m^S=0.431 kg, p^A=2.44 W, m^B=0.144 kg, e^D=164 W.h/kg). The actual measured flight endurance was recorded for two different full cycle test cases. Table I shows the estimated flight endurance, measured mean endurance, standard deviation and the mean error obtained from the experiment. We can see that the estimated flight endurance is accurate, with a mean error of only 0.97 %. These results suggest that the power model for ceiling endurance estimation is realistic and that the assumptions are reasonable.

V. CONCLUSIONS

This paper tackles the energy problem of aerial exploration within indoor environments, first by using ceiling attachment as a means for preserving energy, while still maintaining the birds-eye-view and second by providing a model to estimate the endurance of a hover-capable flying robot. The proposed model for endurance estimation has been extensively tested using a custom-developed quadrotor and ceiling attachment system. The ceiling attachment feature has been successfully demonstrated by flying through several cycles of hovering, attaching to the ceiling, powering off the motors and waiting, re-activating the motors and detaching from the ceiling.

When comparing our model with Valenti and collaborators [6], it is clear that there are benifits in using their model for fault detection. However, if purely flight endurance estimation is considered then the model presented in this paper is much simpler, has a very small error (< 3 %) and has been customised to include perch and stare endurance estimation.

In the future we plan to implement the endurance estimation model on the actual platform to give the platform an 'awareness' of its own avaliable energy. This information could be used by higher-level control strategies for optimising energy resources. We also plan to explore different methods of attaching to non-ferrous ceilings, evaluating systems like, suction, claws, dry adhesives [7], [8], [9], [10] etc. Additionally, it might be interesting to incorporate an automatic recharging system so that the platform can dock to a ceiling based recharging station for fully autonomous operation over long endurace indoor missions.

VI. ACKNOWLEDGMENTS

We would like to thank Peter Dürr for his help with developing the software for battery selection optimisation, Tim Stirling for proof-reading and Antoine Beyeler for his suggestions with graphing. This work is part of the Swarmanoid project, a Future Emerging Technologies (FET IST-022888) project funded by the European commission and the Swiss National Science Foundation.

REFERENCES

[1] S. Bouabdallah, P. Murrieri, and R. Siegwart, "Towards autonomous indoor micro vtol," *Autonomous Robots*, vol. 18, no. 2, pp. 171–183, 2005.

[2] J. C. Zufferey, A. Klaptocz, A. Beyeler, J. D. Nicoud, and D. Floreano, "A 10-gram microflyer for vision-based indoor navigation," in *Proceedings of the IEEE/RSJ International Conference on Intelligent Robots and Systems*, 2006, pp. 3267–3272.

[3] P. Y. Oh, M. J. Joyce, and J. Gallagher, "Designing an aerial robot for hover-and-stare surveillance," *IEEE*, pp. 303–308, 2005.

[4] W. E. Green and P. Oh, "Optic flow based collision avoidance on a hybrid MAV," in *IEEE Robotics and Automation Magazine*, 2008, in Press.

[5] W. E. Green and P. Y. Oh, "Autonomous hovering of a fixed-wing micro air vehicle," in *IEEE International Conference on Robotics and Automation*, 2006, pp. 2164–2169.

[6] M. Valenti, B. Bethke, J.-P. How, D.-P. Farias, and J. Vian, "Embedding health management into mission tasking for uav teams," in *Proceedings of the American Control Conference*, 2007.

[7] O. Unver, A. Uneri, A. Aydemir, and M. Sitti, "Geckobot: A gecko inspired climbing robot using elastomer adhesives," in *Proceedings of the IEEE International Conference on Robotics and Automation*, 2006, pp. 2329–2335.

[8] M. P. Murphy, W. Tso, M. Tanzini, and M. Sitti, "Waalbot: An agile small-scale wall climbing robot utilizing pressure sensitive adhesives," in *IEEE/RSJ International Conference on Intelligent Robots and Systems*, 2006, pp. 3411–3416.

[9] S. Kim, M. Spenko, S. Trujillo, B. Heyneman, V. Mattoli, and M. R. Cutkosky, "Whole body adhesion: hierarchical, directional and distributed control of adhesive forces for a climbing robot," in *IEEE International Conference on Robotics and Automation*, 2007.

[10] K. Autumn, A. Dittmore, D. Santos, M. Spenko, and M. R. Cutkosky, "Frictional adhesion: a new angle on gecko attachment," pp. 3569–3579, 2006.

[11] J. Roberts, T. Stirling, J. C. Zufferey, and D. Floreano, "Quadrotor using minimal sensing for autonomous indoor flight," in *Proceedings of the 3rd US-European Competition and Workshop on Micro Air Vehicles, 7th European Micro Air Vehicle Conference and Flight Competition*, 2007.